X-ray absorption at the oxygen K edge in cubic f oxides examined using a full multiple-scattering approach

1999 J. Phys.: Condens. Matter 11 7185

(http://iopscience.iop.org/0953-8984/11/37/314)

J. Phys.: Condens. Matter **11** (1999) 7185–7194. Printed in the UK PII: S0953-8984(99)04072-2

X-ray absorption at the oxygen K edge in cubic f oxides examined using a full multiple-scattering approach

Z Y Wu†, F Jollet†§, S Gota†, N Thromat†, M Gautier-Soyer† and T Petit‡

† Commissariat à l'Energie Atomique, DSM/DRECAM/SRSIM, Bâtiment 462, CE Saclay, 91191 Gif-sur-Yvette Cédex, France

‡ Commissariat à l'Energie Atomique, DRN/DEC/SECC, 17 rue des Martyrs, 38054 Grenoble Cédex 9, France

Received 7 May 1999, in final form 5 July 1999

Abstract. The O K-edge x-ray absorption near-edge-structure (XANES) spectra of UO_2 and CeO_2 are presented and interpreted. Using different-size clusters around the excited atom in the full multiple-scattering (MS) simulation, we are able to link the features present in the spectra of each oxide to its specific atomic arrangement and electronic structure. The structures at the edge originate from oxygen 2p states hybridized with f and d orbitals of the cation split by the cubic crystal field. All of the other features come from MS with the neighbouring shells of the central oxygen atoms.

1. Introduction

Uranium and cerium dioxides have been widely studied, especially as regards their electronic structure. The occupied states have been analysed by x-ray and resonant photoelectron spectroscopies (XPS and RPS) [1–3] while optical absorption [4] and x-ray absorption spectroscopy (XAS) [5–7] experiments have been performed to obtain information about the empty states of these compounds.

A point of interest concerning these two f oxides is the connection between the electronic structure and the geometric arrangements of the atoms. Indeed, whereas they crystallize in the same cubic symmetry, UO_2 and CeO_2 have very different electronic properties: in an ionic picture U^{4+} has a $5f^2 6d^0$ configuration and Ce^{4+} a $4f^0 5d^0$ one; the two oxides therefore differ in number of f electrons on the cation and in principal quantum number. As Ce^{4+} has an f^0 configuration, CeO_2 is a charge-transfer insulator, while UO_2 is a Mott–Hubbard insulator, the electronic repulsions being responsible for the insulating state [8]. Another interesting point is the participation of the f electrons in the chemical bonding which may be different for the two oxides, the 4f orbitals being more localized than the 5f ones. Indeed, if there is a covalent bonding between oxygen and cation ions, this means that charge transfer has occurred from O^{2-} to M^{4+} (M = U or Ce); the O 2p orbitals have therefore an empty antibonding part due to hybridization with cation empty orbitals, which it is possible to investigate in an O K-edge XANES experiment, as it involves a 1s–2p electronic transition, according to the dipole selection rule. For UO_2 and CeO_2 dioxides, both experimental and theoretical studies

§ Present address: Commissariat à l'Energie Atomique, Centre d'Etudes de Bruyères le Chatel, BP 12, 91680 Bruyères le Chatel Cédex, France.

0953-8984/99/377185+10$30.00

of XANES have concentrated mostly on the cation L and M edges, but the edge of oxygen is still very scarcely examined.

Very recently, these questions have been discussed by some of us in a paper in which a comparison of the oxygen K-edge absorption spectra of UO_2 and CeO_2 is presented and the spectrum of UO_2 is interpreted thanks to first-principles calculations in the framework of the LSDA + U approach [8]. Due to the small size of the atomic basis in such calculations, only the structures close to the absorption edge (the first 10 eV) can be attributed. The relative intensity and the energy separation of e_g and t_{2g} peaks were also not well reproduced. Starting from this work, we present in this paper the interpretation of the characteristic features of the O K-edge spectra for both compounds in the light of full MS calculations using increasing cluster sizes around the excited oxygen atom. In this way we try to connect the specific atomic arrangement and the electronic structure of each oxide with the position, shape, and intensity of the different characteristic features of the spectra. We also present the projected density of states based on the linear muffin-tin orbital atomic sphere approximation (LMTO–ASA) band calculations in order to achieve systematically a better understanding of the bonding and other physical properties.

The paper is organized as follows. Calculation details are presented in section 2 while section 3 is devoted to the presentation of the experimental results. In section 4, the results of the calculation are first discussed for each oxide, and general tendencies are tackled at the end of the paper.

2. Calculational details

Two types of calculation have been performed:

(a) Multiple-scattering (MS) calculations simulating the oxygen absorption spectra. They were carried out on the basis of the one-electron full multiple-scattering (MS) theory [9–13] using the CONTINUUM code [14]. Clusters of increasing size centred on an oxygen emitter atom are first built, on which all the MS events are considered. We have used the Mattheiss prescription [15] to construct the cluster electronic density and the Coulomb part of the potential by superposition of neutral atomic charge densities obtained from the Clementi–Roetti tables [16]. In order to simulate the charge relaxation around the core hole in the photoabsorber of atomic number Z, we have used the screened $Z + 1$ approximation (final-state rule) [17], which consists in taking the orbitals of the $Z+1$ atom and in constructing the final-state charge density by using the excited configuration of the photoabsorber with the core electron promoted to a valence orbital. For practical reasons we use the energy-independent X_α type of exchange followed by a Lorentzian convolution to account for inelastic losses of the photoelectron in the final state and the core-hole width. The total width of the Lorentzian is given by $\Gamma_{tot}(E) = 2\,\mathrm{Im}\,\Sigma(E) + \Gamma_h$ where $\Sigma(E)$ is a volume-averaged value of the Hedin–Lundqvist (H–L) exchange and correlation potential (self-energy) $\Sigma(\vec{r}, E)$ for the unit cell of the compound, as suggested by Penn [18]. We have chosen the muffin-tin radii according to the criterion of Norman [19], and allowed a 10% overlap between contiguous spheres to simulate the atomic bond.

(b) Band-structure (BS) calculations leading to the density of states (DOS) of the compound in the ground state. DOS calculations were performed using density-functional theory (DFT) within the local density approximation (LDA). Here the whole crystal is considered, taking advantage of the periodicity of the mesh. For solving the one-electron Schrödinger equation self-consistently we used the scalar-relativistic LMTO method in the ASA [20]. A detailed description is to be found elsewhere [21].

For UO_2, the DOS are extracted from the LSDA + U calculation detailed in reference [8]. For CeO_2, the same type of calculation has been performed with $U = 0$ as this compound is a charge-transfer insulator, so the LSDA provides a very reasonable starting point, as e.g. for transition metal oxides [22].

3. Results

Uranium and cerium dioxides crystallize in the fluorite structure (CaF_2) and belong to the $Fm3m$ space group. The unit-cell parameter is $a_0 = 5.47$ Å for UO_2 and 5.40 Å for CeO_2. The lattice can be described as a fcc cation lattice in which each of the tetrahedral sites is occupied by an oxygen atom. This leads to a cubic local symmetry around each cation (eight oxygen neighbours located at 2.37 Å in UO_2 and 2.34 Å in CeO_2).

The sample preparation and the experimental conditions have been already given in [23] for CeO_2 and in [8] for UO_2.

Measured oxygen K-edge spectra of UO_2 and CeO_2 are shown in figure 1. We can distinguish two parts in these spectra:

(i) The first one, up to 540 eV, called the edge region, displays four main features labelled a, b, c, and d for UO_2 and three for CeO_2 (labelled b, c, d). For UO_2 the structures are not very well separated. Feature a appears as a small bump on the low-energy side of structure b. Structure b overlaps also with c. In contrast, the three structures for CeO_2 (b, c, d) are very sharp and clearly pronounced.

(ii) The second part, beyond 540 eV, presents four visible structures labelled A, B, C, and D. Their energy positions are listed in table 1. In this region, the two spectra are quite similar although the CeO_2 spectrum is noisier

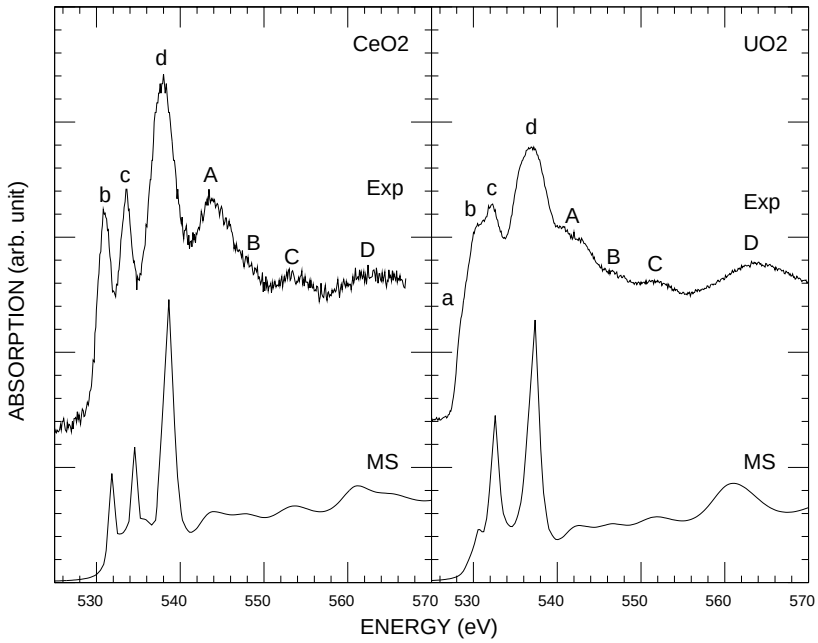

Figure 1. Experimental ('Exp') and multiple-scattering (MS) calculated O K-edge XANES spectra: CeO_2 (left panel) and UO_2 (right panel).

Table 1. The energies of the transition features in the O K-edge spectra for CeO_2 and UO_2 (in eV).

	a	b	c	d	A	B	C	D
UO_2	528.55	530.6	532.2	537.0	542.5	546.8	551.8	564.0
CeO_2		530.9	533.5	537.9	543.0	547.0	553.0	563.0

Figure 1 also contains the MS theoretical calculations of XANES spectra at the O K edge for the two oxides. Size convergence was obtained using a cluster of 125 atoms.

4. Discussion

4.1. UO_2

We have performed MS calculations adding consecutive uranium and oxygen shells around the emitter oxygen atom. The results are shown in figure 2 for five clusters ranging from 5 to 125 atoms. When the convergence is reached, the main peaks of the experimental spectrum are well reproduced: the first three peaks correspond respectively to the b, c, and d experimental structures. The shape of these three peaks is established for a cluster whose size is greater than or equal to 43 atoms. In the fluorite structure, this corresponds to the size where all of the four first uranium neighbours of the central oxygen have all their oxygen first neighbours, with the result that the cubic symmetric environment of the cation sites is achieved. The cubic crystal field is therefore formed and the e_g–t_{2g} splitting clearly appears as shown in the spectra. In

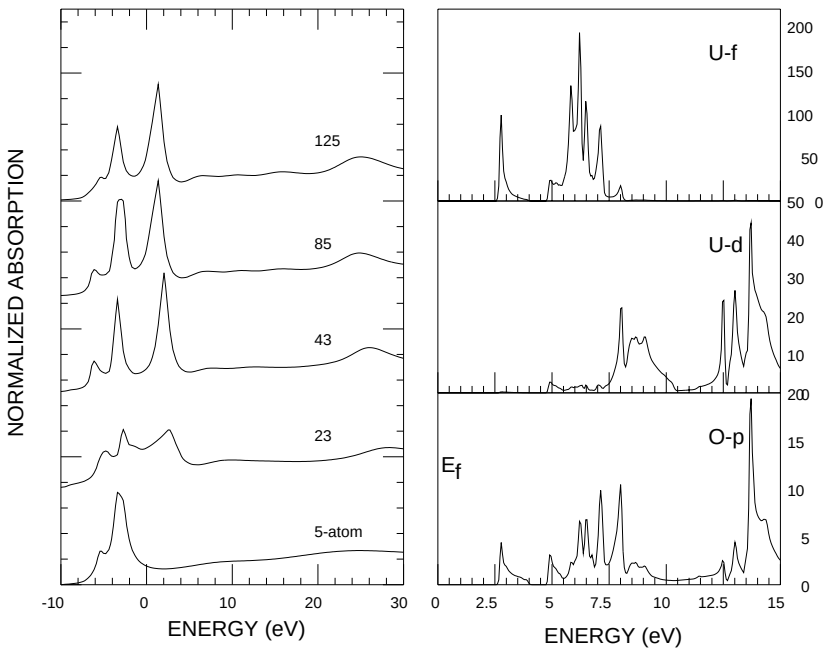

Figure 2. Left panel: the theoretical MS calculation of the O K edge of the UO_2 compound as a function of the cluster size (5, 23, 43, 85, and 125 atoms). Right panel: the projected density of states related to the UO_2 system (reference [8]). The zero of energy corresponds to the Fermi level.

figure 3 we present a simplified 31-atom-cluster (suppressing twelve U atoms at 4.54 Å from the 43-atom cluster) MS calculation, which contains the central oxygen atom, its nearest four U atoms and the outer-shell 26 oxygen atoms that provide an exactly cubic environment for the nearest four U atoms. The peaks b, c, and d are very well defined.

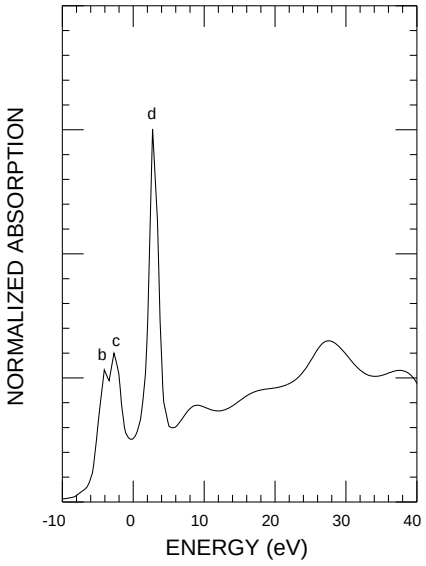

Figure 3. The MS calculation of the O K-edge XANES in UO_2 using a simplified 31-atom cluster: the central oxygen plus the nearest four U and 26 oxygen atoms.

On the basis of MS calculations alone, it is not possible to go further in the interpretation as we cannot distinguish whether peaks come from an O 2p–U 6d or an O 2p–U 5f hybridization. In order to identify the origin of these features, we present in the right-hand panel of figure 2 the partial density of states for UO_2 [8] (BS calculation). The 5f states of uranium in the conduction band are lower in energy than the 6d states, although there is a small overlap between the f and the e_g states, indicating that the spectral features close to the threshold (marked a/b in figure 1) arise from the covalent or hybridization mixing of the oxygen p states with the uranium f density of states. The pronounced doublet feature in the experimental XANES (labelled c and d) is due to the crystal-field splitting of the 6d level into e_g and t_{2g} levels due to the local cubic field around the uranium sites, in agreement with an earlier assignment [8, 24, 25]. The energy separation of this doublet found by MS calculation is about 4.76 eV, which is almost identical with the experimental value (4.8 eV). The structure a cannot be produced in the one-particle approximation as expected, due to the strong 5f–5f-electron correlation in UO_2 ($|\underline{L}5f^3\rangle$ and $|\underline{L}5f^26d^1\rangle$ configurations involved in the final states, where $\underline{L}$ denotes a 1s oxygen hole). This leads to a very complex multiplet structure [8].

The following four structures in the MS region correspond respectively to the A, B, C, and D peaks of the experimental spectrum. They begin to be well reproduced by a 43-atom-cluster MS calculation. Following the procedure for the iron oxides [26], we have calculated the spectra produced by the oxygen shells alone. The results are shown in figure 4, using the same sizes of clusters as were used for figure 2 but suppressing all U atoms, along with the real 125-atom-cluster MS calculation result. The first three spectral features A, B, and C can be attributed to the MS in the cage formed by the oxygen atoms located less than 4.8 Å away from the central absorbing atom, i.e. the first three oxygen shells. Unlike in the case of iron oxides, it is not possible to reproduce the experimental spectra without taking into account the contribution of cations not only for the pre-edge peaks (b, c, and d), which confirms that they

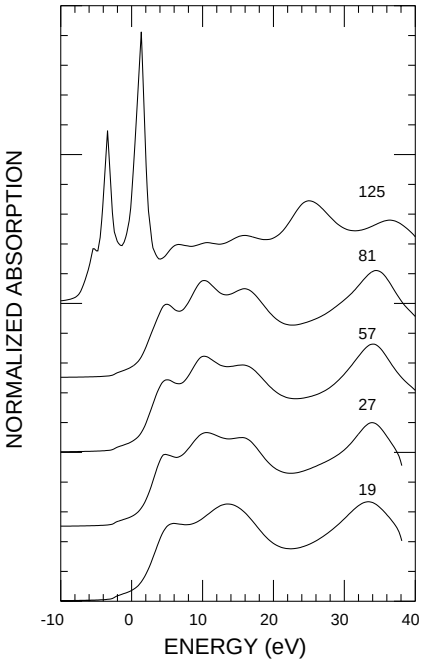

Figure 4. The MS calculation of the O K edge of the UO_2 compound as a function of the cluster size taking into account only oxygen shell contributions (19, 27, 57, and 81 atoms). For comparison, a real 125-atom-cluster calculation is shown at the top.

come from the O–U hybridization, but also for the peak D, which has disappeared. The energy separations among A, B, and C are also changed. This is at variance with the iron oxide case, where all MS peaks were well reproduced by just the oxygen shells. This result demonstrates clearly the fact that the oxygen 2p/metal nd and/or $(n-1)$f interaction becomes stronger for higher atomic numbers due to larger nd/$(n-1)$f orbitals [24].

4.2. CeO_2

The MS calculations of the O K-edge XANES spectra of CeO_2 are reported in figure 5 using the same cluster sizes as were used for UO_2. Qualitatively, one might expect a similar explanation for all the transition features. For a minimal cluster composed of an O central atom (photoabsorber) surrounded by the four nearest-neighbouring Ce atoms, the calculated absorption spectrum already shows the presence of the pre-edge peaks b and c which can be attributed to the transition to O 2p states hybridized with the Ce 4f and 5d states, respectively, mainly localized at the Ce site [25]. This is verified by DOS calculations as shown in the right-hand panel: the first peak in the O p-projected DOS is mainly due to the hybridization with Ce f orbitals; the peaks c and d are attributed to the contribution of average e_g and t_{2g} band-like states. The 'crystal-field' splitting is reproduced by MS calculations when using large clusters (43, 85, and 125 atoms). In the same way as we did for UO_2, we present in figure 6 a simplified 31-atom cluster (obtained from a 43-atom cluster by suppressing twelve Ce at 4.49 Å) which contains enough oxygen atoms to form the exact cubic environment of the nearest Ce atoms. The peaks b, c, and d are very well defined, further confirming that their presence is to be associated with the existence of unoccupied states made up of O 2p orbitals mixed with Ce 4f and Ce 5d orbitals. The energy separation of c and d is about 4.10 eV, which is in good agreement with the 4.30 eV experimental value. Peaks b, c, and d are sharper for CeO_2, reflecting weaker multiplet f and d splittings than those for UO_2.

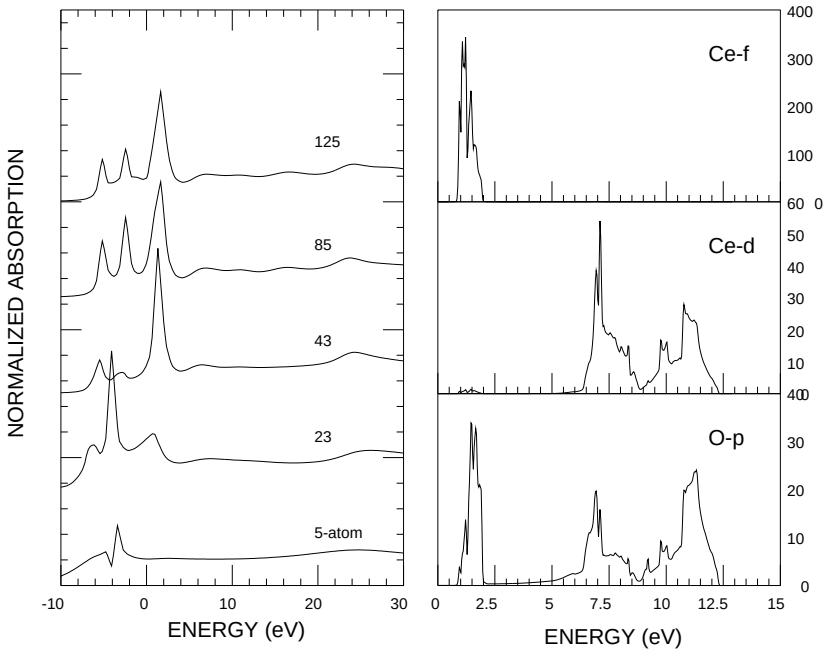

Figure 5. Left panel: the MS calculation of the O K edge of the CeO_2 compound as a function of the cluster size (5, 23, 43, 85, and 125 atoms). Right panel: the projected density of states related to the CeO_2 system. The zero of energy corresponds to the Fermi level.

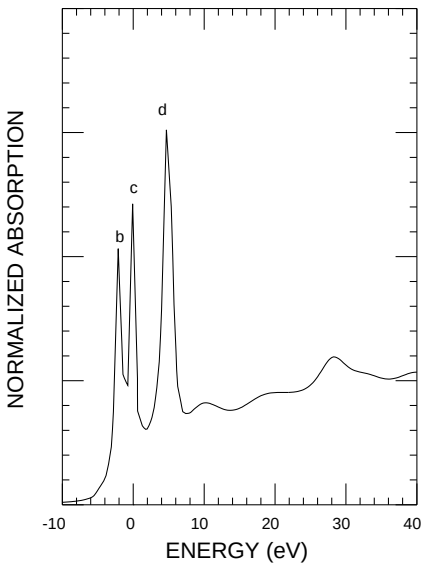

Figure 6. The MS calculation of the O K-edge XANES in CeO_2 using a simplified 31-atom cluster: the central oxygen plus the nearest four U and 26 oxygen atoms.

The spectrum, in the first 10 eV, made up of three sharp peaks, shows considerable differences compared to the spectrum of UO_2 presented on figure 2, reflecting the difference in electronic structure of the two compounds. Indeed, for CeO_2 one has to consider the $4f^1$ final state only—the cubic crystal field on the f orbitals can be neglected—and the $4f^1$ states

are made up of a sharp peak b, shown in the spectrum. The rest of the spectrum appears to be similar to that of UO_2; this arises from the fact that the two compounds have the same crystalline structures. In figure 7 we present the contributions of the oxygen atoms only, with the 125-atom real-cluster calculation. The energy positions and intensities of the four spectral structures A, B, C, and D are quite different for the 81-oxygen and the 125-atom-cluster results, indicating that Ce atoms play an important role in the MS region of the XANES spectrum due to the strong covalency between Ce and O atoms.

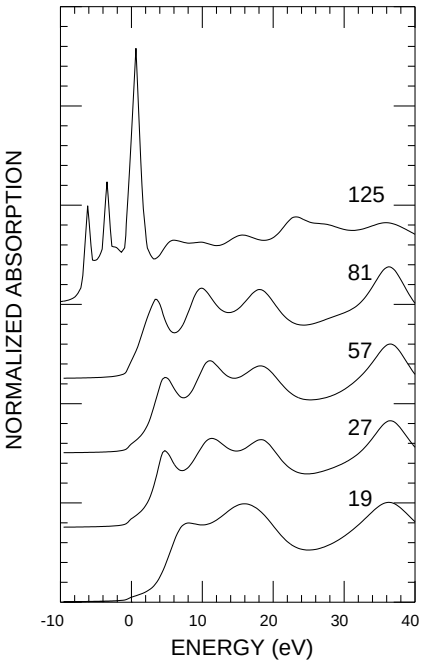

Figure 7. The MS calculation of the O K edge of the CeO_2 compound as a function of the cluster size taking into account only oxygen shell contributions (19, 27, 57, and 81 atoms). For comparison, a 125-atom real-cluster MS calculation is shown at the top.

4.3. The core-hole potential

We present in figure 8 a comparison between the fully relaxed final-state (in the $Z + 1$ approximation) and the ground-state (GS) potential calculations. The results are quite similar for the two different potential calculations, except the small difference in the relative intensities of the pre-edge features. This is because the core hole is now located on the oxygen while the states in the unoccupied bands just above the Fermi level have most weight on the cation site, indicating that the spectrum is rather insensitive to the core-hole potential effects.

5. Conclusions

The MS calculations presented here reproduce well all the experimental structures of the O K XANES spectrum for UO_2 and CeO_2. The shell-by-shell MS calculations, associated with LMTO–ASA DOS calculations, allow us to clearly distinguish two parts in the spectra:

(a) The first one ranges from the edge to 540 eV. The features present in this part are a fingerprint of the electronic structure of the cation in the local crystal field. They correspond to the lowest-energy states in the conduction band, projected on the local oxygen p states. The interplay between crystal-field effects, 4f, 5d (or 5f, 6d) interactions,

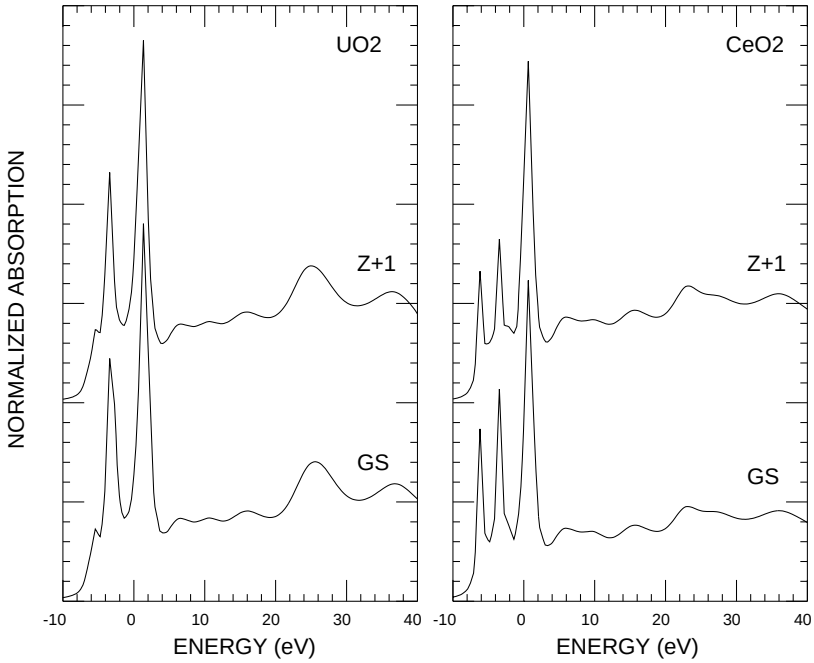

Figure 8. Comparison between two MS calculations at the oxygen K edge made using two different final-state potentials: the $Z+1$ final-state potential and the ground-state (GS) potential. Right panel: UO_2; left panel: CeO_2.

as well as multiplet structure, are responsible for the different features of the spectra. As the cubic crystal field is identical in the two structures, the differences between the two spectra essentially come from the different cation local electronic structure. As already established in reference [8], the UO_2 spectrum is characterized in this part of the spectrum by short-range (first-neighbour) interactions including e_g–t_{2g} splitting induced by the local cubic d crystal field (features c, d) and hybridization of O 2p and U 5f states strongly influenced by the complex multiplet f structure of the cation (features a, b). The difference between the spectra in this energy range comes mainly from features a and b; it is shown thanks to band-structure calculations that this reveals a difference in f multiplet structure between the two cations.

(b) The second one, beyond 540 eV, is very similar for the two spectra. The features present in this part, that can be calculated only thanks to MS calculations, essentially reflect the mean range order, which is the same in the two structures. They can therefore be considered as a fingerprint of the geometrical structure of several shells of neighbours of the emitter oxygen atom. They come from MS paths involving both the oxygen atoms and the cations, emphasizing the role of heavy cations as compared with lighter ones as in iron oxides [26].

Thanks to adequate calculations, it is therefore possible to discriminate in the XANES spectra the features which are related to short-range interactions, mainly driven by the electronic structure in one part of the spectra, and the ones coming from the mean-range geometrical structure in the other part.

References

[1] Baer Y and Schoenes J 1980 *Solid State Commun.* **33** 885
[2] Gunnarsson O, Sarma D D, Hillebrecht F U and Schönhammer K 1988 *J. Appl. Phys.* **63** 3676
[3] Cox L E, Ellis W P, Cowan R D, Allen J W, Oh S J, Lindau I, Pate B B and Arko A J 1987 *Phys. Rev.* B **35** 5761 and references therein
[4] Schoenes J 1980 *J. Physique Coll.* **41** C5 31
[5] Guo J, Ellis D E, Alp E, Soderholm L and Shenoy G K 1989 *Phys. Rev.* B **39** 6125
[6] Hudson E A, Rehr J J and Bucher J J 1995 *Phys. Rev.* B **52** 13 815 and references therein
[7] Petiau J, Calas G, Petitmaire D, Bianconi A, Benfatto M and Marcelli A 1986 *Phys. Rev.* B **34** 7350
[8] Jollet F, Petit T, Gota S, Thromat N, Gautier-Soyer M and Pasturel A 1997 *J. Phys.: Condens. Matter* **9** 9393
[9] Stöhr J 1988 *X-Ray Absorption: Principles, Applications, Techniques of EXAFS, SEXAFS, XANES* ed R Prinz and D Koningsberger (New York: Wiley) p 443
[10] Durham P J 1988 *X-ray Absorption: Principles, Applications, Techniques of EXAFS, SEXAFS, XANES* ed R Prinz and D Koningsberger (New York: Wiley)
[11] Lee P A and Pendry J B 1975 *Phys. Rev.* B **11** 2795
[12] Natoli C R, Misemer D K, Doniach S and Kutzler F W 1980 *Phys. Rev.* A **22** 1104
Natoli C R and Benfatto M 1986 *J. Physique Coll.* **47** C8 11
Natoli C R, Benfatto M and Doniach S 1986 *Phys. Rev.* B **34** 4682
Natoli C R, Benfatto M, Brouder C, Ruiz Lopez M Z and Foulis D L 1990 *Phys. Rev.* B **42** 1944
[13] Wu Z Y, Benfatto M and Natoli C R 1992 *Phys. Rev.* B **45** 531
Wu Z Y, Benfatto M and Natoli C R 1993 *Solid State Commun.* **87** 475
[14] Natoli C R 1990 unpublished
[15] Mattheiss L 1964 *Phys. Rev.* A **134** 970
[16] Clementi E and Roetti C 1974 *At. Data Nucl. Data Tables* **14** 177
[17] Lee P A and Beni G 1977 *Phys. Rev.* B **15** 2862
[18] Penn D R 1987 *Phys. Rev.* B **35** 482
[19] Norman J G 1974 *Mol. Phys.* **81** 1191
[20] Andersen O K 1975 *Phys. Rev.* B **12** 3060
Andersen O K and Jepsen O 1984 *Phys. Rev. Lett.* **53** 2571
Andersen O K, Jepsen O and Sob M 1986 *Electronic Band Structure and its Applications* ed M Yussouff (Berlin: Springer)
Jepsen O and Andersen O K 1995 *Z. Phys.* B **97** 35
Lambrecht W R and Andersen O K 1986 *Phys. Rev.* B **34** 2439
Blöchl P E, Jepsen O and Andersen O K 1994 *Phys. Rev.* B **49** 16 223
[21] Skriver H L 1984 *The LMTO Method* (Berlin: Springer)
Fuggle J C and Inglesfield J E (ed) 1992 *Unoccupied Electronic States (Springer Topics in Applied Physics vol 69)* chs 2, 3, 5
Van Schilfgaarde M, Paxton A T and Methfessel M 1994 *LMTO–ASA Program version 4.1*
[22] Sarma D D, Shanthi N, Barman S R, Hamada N, Sawada H and Terakura K 1995 *Phys. Rev. Lett.* **75** 1126
[23] Douillard L, Gautier-Soyer M, Thromat N, Henriot M, Guittet M J, Duraud J P and Tourillon G 1994 *Phys. Rev.* B **49** 16 171
[24] Soriano L, Abbate M, Fuggle J C, Jimenez M A, Sanz J M, Mythen C and Padmore H A 1993 *Solid State Commun.* **87** 699
[25] de Groot F M F, Grioni M, Fuggle J C, Ghijsen J, Sawatzky G A and Petersen H 1989 *Phys. Rev.* B **40** 5715
[26] Wu Z Y, Gota S, Jollet F, Pollak M, Gautier-Soyer M and Natoli C R 1997 *Phys. Rev.* B **55** 2570